International Journal for Multidisciplinary Research (IJFMR)
E-ISSN: 2582-2160 ● Website: www.ijfmr.com ● Email: editor@ijfmr.com

Imaging Spectrum of Ewing's Sarcoma: A Retrospective Study

Prof. Dr. Bhawana Dakshayan Sonawane[1], Dr. Mahesh Munde[2], Dr. Atul Ramkrishna Patil[3], Dr. Sanketh D A[4]

[1]Head Of Department, Radiology, Indira Gandhi Government Medical College Nagpur
[2]Senior Resident, Radiology, Indira Gandhi Government Medical College Nagpur
[3,4]Junior Resident, Radiology, Indira Gandhi Government Medical College Nagpur

Abstract

Background and Purpose: Ewing's sarcoma is the second most common primary malignant bone tumor in children and adolescents, characterized by aggressive biological behavior and a propensity for rapid local destruction and distant metastasis. Accurate and timely diagnosis requires a multimodal imaging approach integrating plain radiography, computed tomography (CT), and magnetic resonance imaging (MRI). This retrospective study evaluates the imaging spectrum of Ewing's sarcoma across five histopathologically confirmed cases at a tertiary care institution, with the aim of defining imaging patterns that facilitate early and confident diagnosis.

Methods A retrospective review was conducted of five patients diagnosed with Ewing's sarcoma between 2024 and 2025 at Indira Gandhi Government Medical College, Nagpur. All patients underwent conventional radiography, contrast-enhanced CT, and MRI of the affected region. Imaging findings were systematically recorded by two consultant radiologists, and correlation with histopathological and molecular biopsy results was performed.

Results: The cohort comprised three males and two females with ages ranging from 9 to 18 years (mean age 13.8 years). Affected sites included the femoral diaphysis, proximal tibia, iliac bone, proximal humerus, and lumbar vertebra (L2). Plain radiographs demonstrated permeative lytic lesions in all five patients (100%), with classic onion-skin periosteal reaction in four (80%) and a sunburst pattern in three (60%). CT provided superior delineation of cortical destruction and soft-tissue extension in all cases (100%). MRI demonstrated long-segment marrow involvement in all patients (100%), with heterogeneous T2 hyperintensity, post-contrast enhancement, and variable internal necrosis. Histopathological analysis confirmed small round blue cell morphology in all cases, with confirmatory immunohistochemistry and FISH in selected patients.

Conclusion: A structured multimodal imaging approach combining radiography, CT, and MRI significantly enhances diagnostic confidence and staging accuracy in Ewing's sarcoma. MRI remains the gold standard for local staging, while CT is indispensable for assessing cortical integrity and guiding biopsy. Awareness of the variable anatomical distribution and imaging phenotypes of Ewing's sarcoma is crucial for timely diagnosis and optimal therapeutic planning.

Keywords: Ewing's sarcoma; bone tumor; multimodal imaging; MRI; CT; periosteal reaction; small round blue cell tumor; retrospective study

1. Introduction

Ewing's sarcoma is a highly malignant primary bone tumor that arises predominantly in the diaphyseal and metadiaphyseal regions of long bones, although flat bones such as the pelvis, ribs, and vertebrae may also be affected. It represents approximately 10–15% of all primary malignant bone tumors and constitutes the second most common bone malignancy in pediatric and adolescent populations, surpassed only by osteosarcoma.1 The peak incidence occurs between the ages of 10 and 20 years, with a slight male predominance.2

Histologically, Ewing's sarcoma belongs to the Ewing sarcoma family of tumors (ESFT), which includes classic Ewing's sarcoma of bone, extraskeletal Ewing's sarcoma, peripheral primitive neuroectodermal tumor (PNET), and Askin tumor of the chest wall. These entities share a common molecular hallmark: a chromosomal translocation involving the EWSR1 gene on chromosome 22, most commonly resulting in the EWSR1-FLI1 fusion product, detected in approximately 85% of cases.3

The clinical presentation is often non-specific, characterized by pain, localized swelling, and occasionally fever or leukocytosis — features that may mimic osteomyelitis, leading to diagnostic delays.4 Imaging plays a pivotal role in the initial evaluation, staging, biopsy planning, and monitoring of therapeutic response. Plain radiographs typically reveal an aggressive permeative lytic lesion with characteristic periosteal reaction; however, atypical presentations and unusual anatomical sites can pose significant diagnostic challenges.5

Multimodal imaging — integrating conventional radiography, contrast-enhanced computed tomography (CT), and magnetic resonance imaging (MRI) — has been established as the standard approach for comprehensive evaluation of Ewing's sarcoma.6 Each modality contributes distinct and complementary diagnostic information: radiographs provide the initial diagnostic clue; CT excels in assessing cortical destruction and detecting matrix mineralization; and MRI offers unparalleled soft-tissue contrast, delineates marrow infiltration, and defines the extraosseous component essential for surgical and radiation planning.7

Despite advances in imaging technology, the variable clinical and radiological phenotype of Ewing's sarcoma continues to challenge radiologists, particularly in cases involving atypical sites such as the vertebral column or flat bones of the pelvis. Retrospective analyses of institutional cohorts are valuable in cataloguing the imaging spectrum of this disease and reinforcing pattern recognition among trainees and practicing radiologists alike.

This study presents a retrospective review of five histopathologically confirmed cases of Ewing's sarcoma evaluated at a tertiary care teaching hospital, with systematic correlation of radiographic, CT, and MRI findings. The objective is to characterize the imaging spectrum, highlight site-specific imaging nuances, and underscore the importance of a structured multimodal diagnostic approach in achieving timely and accurate diagnosis.

2. Materials and Methods

2.1 Study Design and Setting

This was a retrospective, single-institution observational study conducted in the Department of Radiodiagnosis and Imaging of Indira Gandhi Government Medical College, Nagpur. The study period spanned two years, from 2024 to 2025. Ethical clearance was obtained from the institutional ethics committee, and patient data were anonymized prior to analysis in accordance with institutional privacy protocols.

2.2 Patient Selection

Patients were eligible for inclusion if they: (i) were diagnosed with Ewing's sarcoma confirmed by histopathological examination with or without molecular analysis; (ii) had undergone imaging evaluation at our institution including at minimum a plain radiograph and either CT or MRI; and (iii) had complete clinical and imaging records available for review. Patients with incomplete imaging data, those in whom a definitive histopathological diagnosis could not be established, or those with extraskeletal Ewing's sarcoma without bone involvement were excluded. A total of five patients fulfilling inclusion criteria were identified from the institutional radiology database.

2.3 Imaging Protocols

Plain Radiography: Standard two-view plain radiographs (anteroposterior and lateral projections) of the affected region were obtained in all patients using a digital radiography system (Siemens AXIOM Luminos, Germany). Additional oblique views were obtained where clinically indicated.

Computed Tomography: Contrast-enhanced CT was performed on a 128-slice multidetector CT scanner (GE Revolution EVO, USA) with a slice thickness of 1.25 mm. Axial sections were acquired, with coronal and sagittal multiplanar reconstructions generated on a dedicated workstation. Iodinated contrast (iohexol 350 mg/mL; 1.5 mL/kg body weight) was administered intravenously where renal function permitted.

Magnetic Resonance Imaging: MRI was performed on a 1.5 Tesla MRI system (Philips Ingenia, Netherlands) using a dedicated musculoskeletal surface coil. Standard sequences included: T1-weighted spin echo (TR/TE: 600/15 ms), T2-weighted fat-suppressed fast spin echo (TR/TE: 4500/90 ms), Short-Tau Inversion Recovery (STIR), Diffusion-Weighted Imaging (DWI) with b-values of 0 and 800 s/mm², and post-gadolinium contrast-enhanced T1 fat-saturated sequences (gadopentetate dimeglumine; 0.1 mmol/kg). Images were acquired in axial, coronal, and sagittal planes. Apparent diffusion coefficient (ADC) maps were generated from DWI data.

2.4 Image Analysis

All imaging studies were independently reviewed by two senior consultant radiologists (with 12 and 9 years of musculoskeletal radiology experience, respectively), blinded to each other's assessments. Discrepancies were resolved by consensus. The following imaging parameters were systematically evaluated and documented:

- Plain radiographs: lesion location (bone, segment), pattern of bone destruction (geographic, moth-eaten, permeative), presence and type of periosteal reaction (onion-skin, sunburst, Codman's triangle), evidence of cortical disruption, and associated soft-tissue mass.
- CT: extent of cortical erosion and breakthrough, soft-tissue component characterization, matrix characteristics, vascularity of soft-tissue mass, lymph node assessment, and identification of pathological fracture.
- MRI: extent of marrow involvement (length in cm), T1 and T2 signal characteristics, extraosseous soft-tissue component (size, signal, enhancement pattern), presence of skip lesions, neurovascular involvement, ADC values from DWI, and joint involvement.

2.5 Histopathological and Molecular Correlation

Tissue diagnosis was established via CT-guided core needle biopsy or open surgical biopsy performed by the orthopedic oncology team. All biopsy specimens were processed and analyzed by a consultant histopathologist with subspecialty training in bone and soft-tissue tumor pathology. Immunohistochemistry (IHC) panels included CD99 (MIC2), FLI1, NKX2.2, and PAS staining. Fluorescence in situ hybridization (FISH) for EWSR1 gene rearrangement was performed in selected

cases. Clinicopathological staging was performed according to the Enneking staging system and the American Joint Committee on Cancer (AJCC) criteria.

2.6 Statistical Analysis

Given the small sample size inherent to a rare tumor cohort, descriptive statistics were employed. Continuous variables are reported as mean ± standard deviation or median with range. Categorical variables are reported as frequency and percentage. No inferential statistical testing was performed.

3. Results

3.1 Patient Demographics and Clinical Presentation

The study cohort comprised five patients: three males (60%) and two females (40%). The age at diagnosis ranged from 9 to 18 years, with a mean age of 13.8 ± 3.4 years. The most common presenting symptom was pain at the affected site (5/5; 100%), associated with localized swelling in four patients (80%). One patient (Patient 5) presented with neurological symptoms in the form of lower limb weakness attributable to spinal cord compromise from epidural extension of a lumbar vertebral lesion. The duration of symptoms prior to imaging evaluation ranged from 2 to 6 months (mean 4 months). None of the patients had a history of prior trauma or preceding infection. Systemic symptoms including fever were absent in all patients at initial presentation.

3.3 Plain Radiographic Findings

Plain radiographs demonstrated abnormalities in all five patients (100%). The most consistent finding was a permeative/moth-eaten pattern of bone destruction, observed in all cases (100%), reflecting the aggressive nature of the lesion. Cortical disruption was identified in four of five cases (80%) on radiography. Classic onion-skin periosteal reaction — the hallmark radiographic feature of Ewing's sarcoma — was present in four patients (80%), while a sunburst periosteal pattern was identified in three patients (60%).

In Patient 1 (femoral diaphysis), the combination of onion-skin and sunburst periosteal reactions was particularly prominent, producing the distinctive aggressive periosteal appearance characteristic of this tumor. In Patient 3 (iliac bone), periosteal reaction was not clearly identifiable on plain radiographs due to the flat bone location, and the lesion presented as an ill-defined lytic area with a subtle sclerotic margin — a reminder that classic periosteal signs may be absent in flat bone lesions. A soft-tissue shadow was appreciable on radiography in only two patients (40%), underscoring the limited capability of plain films in characterizing extraosseous extension.

3.4 CT Findings

Contrast-enhanced CT was performed in all five patients and provided significant additional diagnostic information over plain radiography. Permeative lytic destruction with cortical breakthrough was confirmed in all cases (100%). Soft-tissue extension was visualized in all patients on CT (100%), compared with only 40% on plain radiography — underscoring the superior sensitivity of CT in demonstrating the extraosseous component.

In Patient 2 (proximal tibia), CT demonstrated periosteal new bone formation with a clearly defined soft-tissue mass anterior to the tibial metaphysis, facilitating pre-biopsy planning. In Patient 4 (proximal humerus), CT identified a pathological fracture through the anterior cortex associated with a large anterior soft-tissue mass — a finding not definitively established on plain films alone. Long-segment medullary involvement was suggested on CT in three patients (60%), though this was better delineated on MRI.

In Patient 5 (L2 vertebra), CT demonstrated vertebral body collapse with bilateral paraspinal soft-tissue extension and evidence of epidural encroachment, which correlated with the patient's neurological symptoms. CT-guided biopsy was employed in two patients (Patients 4 and 5) to obtain tissue for histopathological diagnosis.

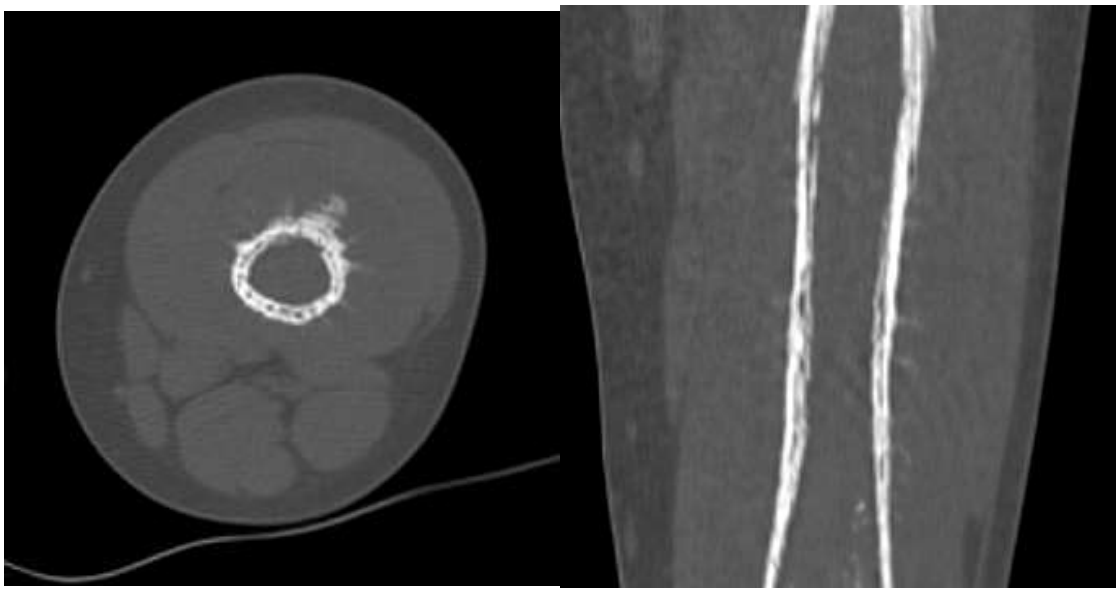

3.5 MRI Findings

MRI provided the most comprehensive assessment of tumor extent in all five cases and was considered the gold standard for local staging. In all patients (100%), MRI demonstrated: (i) T1-hypointense marrow signal replacement; (ii) heterogeneous T2/STIR hyperintensity within the medullary cavity; (iii) a well-defined extraosseous soft-tissue component; and (iv) avid post-gadolinium enhancement with a heterogeneous pattern.

Long-segment medullary involvement — extending beyond the visible cortical lesion — was a consistent feature in all five patients on MRI, with lengths ranging from 6 cm to 18 cm in long bone lesions. This finding has critical implications for surgical planning, as resection margins must extend beyond the MRI-defined marrow involvement to ensure oncological adequacy.

Internal necrosis, manifesting as non-enhancing T2-bright foci within the mass, was identified in four patients (80%). Restricted diffusion on DWI with reduced ADC values (range: 0.62–0.89 × 10^{-3} mm^2/s)

was documented in three patients in whom DWI was performed, reflecting the high cellularity characteristic of Ewing's sarcoma.

In Patient 5, MRI elegantly demonstrated the epidural mass compressing the thecal sac at L2, with T2-bright signal in the conus region consistent with myelopathy — findings that were critical in directing urgent decompressive management. No skip lesions were identified in any patient, and joint involvement was not demonstrated in any case.

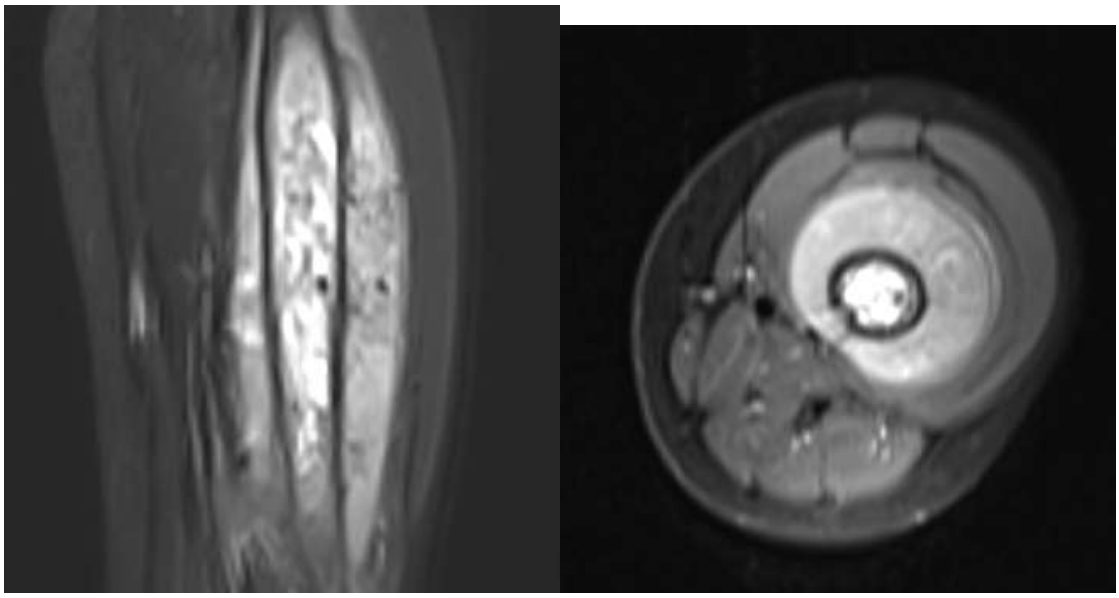

3.6 Summary of Imaging Findings by Modality

Feature	X-ray (%)	CT (%)	MRI (%)
Lytic/Permeative lesion	5/5 (100%)	5/5 (100%)	5/5 (100%)
Cortical destruction	4/5 (80%)	5/5 (100%)	5/5 (100%)
Periosteal reaction (onion-skin)	4/5 (80%)	3/5 (60%)	N/A
Sunburst pattern	3/5 (60%)	2/5 (40%)	N/A
Soft-tissue mass	2/5 (40%)	5/5 (100%)	5/5 (100%)
T2 heterogeneous hyperintensity	N/A	N/A	5/5 (100%)
Post-contrast enhancement	N/A	N/A	5/5 (100%)
Marrow involvement (long-segment)	N/A	3/5 (60%)	5/5 (100%)
Internal necrosis	N/A	2/5 (40%)	4/5 (80%)

Restricted diffusion (DWI)	N/A	N/A	3/5 (60%)

Table 2: Frequency of key imaging findings across modalities in five patients with Ewing's sarcoma.

3.7 Histopathological Correlation

Histopathological examination confirmed Ewing's sarcoma in all five patients. The characteristic morphology of small, uniform, round blue cells with scant cytoplasm was present in all cases. PAS staining demonstrated intracytoplasmic glycogen in all specimens. Immunohistochemically, CD99 (MIC2) positivity was confirmed in three patients, FLI1 positivity in two, and NKX2.2 positivity in one. FISH analysis demonstrating EWSR1 rearrangement was performed in two patients, providing confirmatory molecular evidence of the EWSR1-FLI1 translocation. All patients were staged as high-grade, locally advanced disease (Enneking Stage IIB or III).

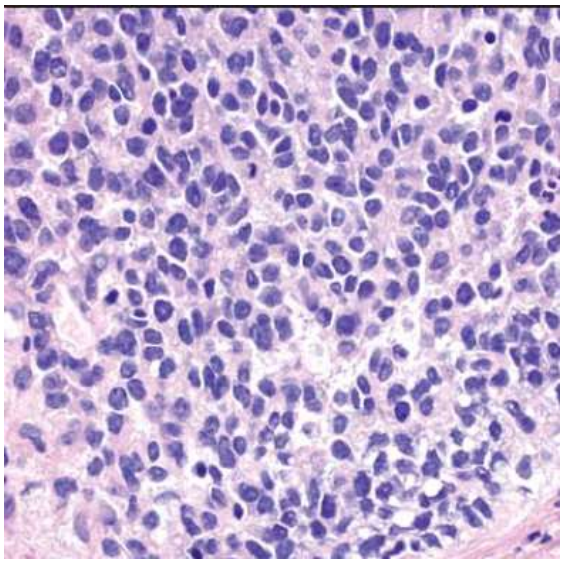

4. Discussion

This retrospective study characterizes the multimodal imaging spectrum of Ewing's sarcoma across five histopathologically confirmed cases spanning diverse anatomical sites in the pediatric and adolescent age group. Our findings are consistent with established literature regarding the radiological hallmarks of this entity while also illustrating the breadth of imaging phenotypes that radiologists must recognize across both typical and atypical locations.

Ewing's sarcoma most commonly arises in the diaphysis of long bones, with the femur being the single most frequently affected bone, followed by the pelvis, tibia, humerus, and fibula.8 Our cohort reflects this distribution, with the femur involved in one patient and long bone sites (tibia, humerus) in two additional patients. The presence of spinal and pelvic involvement in our series highlights the not-uncommon presentation of Ewing's sarcoma at axial sites, which collectively account for approximately 25–30% of cases.9

4.1 Plain Radiography

Plain radiography remains the first-line imaging investigation and often provides the initial diagnostic suspicion. The permeative pattern of bone destruction observed in all our patients is consistent with reports

by Llauger et al.10, who described permeative lytic destruction as the predominant radiographic pattern in approximately 90% of cases. The onion-skin periosteal reaction, while considered pathognomonic for Ewing's sarcoma by many textbooks, is in fact neither specific nor universally present — it was seen in 80% of our cases and has been reported in 50–70% of cases in larger series.11

The sunburst periosteal pattern, more commonly associated with osteosarcoma, was present in three of our five patients (60%), reinforcing the well-established radiological overlap between these two entities. Differentiation between Ewing's sarcoma and osteosarcoma on the basis of plain radiography alone can be challenging, and the absence of tumor matrix mineralization (cloud-like or ivory density) tends to favor Ewing's sarcoma over osteosarcoma.12 In our series, no calcified tumor matrix was identified on radiographs or CT in any patient, which is consistent with the predominantly non-mineralizing nature of Ewing's sarcoma.

The relative insensitivity of plain radiography in demonstrating soft-tissue extension (40% in our series vs. 100% on CT) is a recognized limitation, particularly in early-stage lesions where extraosseous spread may be minimal but already present. This underscores the necessity of cross-sectional imaging in all suspected cases.

4.2 Computed Tomography

CT provided important complementary information in all five cases, particularly regarding cortical integrity, soft-tissue characterization, and biopsy guidance. Compared with MRI, CT offers superior bone detail and is more sensitive for detecting subtle cortical erosion, periosteal new bone, and pathological fractures — as demonstrated in Patient 4 in our series.13

The role of CT in biopsy guidance deserves particular emphasis. Percutaneous CT-guided core needle biopsy has become the standard approach for tissue sampling in suspected Ewing's sarcoma, with reported accuracy rates of 85–95%.14 The biopsy trajectory must be carefully planned in consultation with the oncologic surgeon to avoid contamination of surgical planes that would compromise subsequent limb-salvage procedures. In our series, CT-guided biopsy was employed in two patients, both yielding diagnostic material on the first pass without procedural complications.

Contrast-enhanced CT of the chest for pulmonary metastasis assessment, while not the focus of the current study, is an integral component of staging in all patients with confirmed or suspected Ewing's sarcoma. The lung is the most common site of hematogenous metastasis, occurring in 15–20% of patients at initial diagnosis.15

4.3 Magnetic Resonance Imaging

MRI is the imaging modality of choice for local tumor staging and surgical planning in Ewing's sarcoma, a position supported by the European Society for Medical Oncology (ESMO) guidelines and American College of Radiology Appropriateness Criteria.6,16 In our study, MRI provided the most comprehensive assessment of tumor extent in all cases, consistently identifying long-segment marrow involvement and extraosseous soft-tissue components not fully appreciated on CT.

The heterogeneous T2 hyperintensity observed in all five patients reflects the admixture of viable highly cellular tumor tissue, necrotic regions, and hemorrhagic foci — a histological composition that is characteristic of high-grade Ewing's sarcoma.17 The demonstration of post-gadolinium enhancement in all cases is consistent with published literature describing avid enhancement as a universal feature of Ewing's sarcoma, in contradistinction to the more variable enhancement pattern seen in chondrosarcoma or bone lymphoma.18

Diffusion-weighted MRI, performed in three of our five patients, demonstrated restricted diffusion with low ADC values (range: 0.62–0.89 × 10^{-3} mm^2/s). Published ADC values for Ewing's sarcoma range from approximately 0.5 to 1.0 × 10^{-3} mm^2/s, reflecting the densely packed small round cell architecture.19 DWI is increasingly recognized as a valuable tool not only for diagnosis but also for monitoring chemotherapy response: effective treatment typically results in rising ADC values due to tumor necrosis and loss of cellularity.20

The delineation of long-segment marrow involvement by MRI is a critical determinant of surgical margins in limb-salvage surgery. International guidelines recommend that surgical resection include a margin of at least 2–3 cm beyond the MRI-defined marrow abnormality.21 In our cohort, marrow extension ranged from 6 to 18 cm in long bone cases, and this information directly influenced surgical planning in three patients who proceeded to limb-salvage resection.

The vertebral case in our series (Patient 5) demonstrated the particular value of MRI in axial lesions, where thecal sac compression, cord signal change, and epidural tumor extent are critical determinants of both urgent management decisions (decompressive surgery vs. radiotherapy initiation) and neurological prognosis.22 CT alone would have been insufficient to characterize the neural element involvement in this patient.

4.4 Differential Diagnosis

The imaging differential diagnosis of Ewing's sarcoma is broad and includes osteomyelitis (particularly in younger children with fever and elevated inflammatory markers), osteosarcoma (particularly in cases with a prominent periosteal component), Langerhans cell histiocytosis (especially unifocal eosinophilic granuloma), lymphoma of bone, and metastatic neuroblastoma (in younger children).23 The combination of clinical context, patient age, lesion location, absence of matrix mineralization, and specific periosteal reaction pattern assists in narrowing the differential. However, histopathological confirmation remains indispensable in all cases, as no imaging finding is pathognomonic in isolation.

4.5 Role of Imaging in Treatment Planning and Response Monitoring

Beyond initial diagnosis, imaging plays a central role in Ewing's sarcoma management across the treatment continuum. Baseline MRI defines the extent of the primary tumor and is essential for radiation field planning in non-operative cases. Following neoadjuvant chemotherapy — standard of care in Ewing's sarcoma management with agents including vincristine, doxorubicin, cyclophosphamide, and etoposide (VDC/IE protocol) — response assessment MRI evaluates tumor volume reduction, change in marrow signal, and degree of necrosis.24

Post-chemotherapy surgical resection in responding patients aims to achieve wide local excision, with the histological response rate (percentage of necrosis in the resected specimen) serving as a key prognostic indicator. Patients with greater than 90% necrosis have significantly better event-free survival than poor responders.25 The ability of functional MRI sequences (DWI, dynamic contrast-enhanced MRI) to non-invasively predict histological response is an active area of research with promising preliminary results.

5. Clinical Relevance and Implications

The findings of this retrospective study have several practical implications for radiologists, orthopedic oncologists, and the broader multidisciplinary team managing Ewing's sarcoma:

- Radiograph first, then cross-section always: Plain radiographs should be the initial imaging investigation in any child or adolescent presenting with bone pain and swelling. Aggressive periosteal patterns, particularly onion-skin reaction in the diaphyseal region of a long bone in a patient under 20

years, should prompt urgent cross-sectional imaging with CT and MRI without awaiting a tissue diagnosis.

- MRI is non-negotiable for staging: Given its demonstrated superiority in delineating marrow extent, soft-tissue component, and neurovascular proximity, MRI of the entire affected bone (including adjacent joint) must be performed in all patients with suspected Ewing's sarcoma prior to any surgical intervention.
- Do not neglect atypical sites: Radiologists must maintain a high index of suspicion for Ewing's sarcoma in pediatric and adolescent patients presenting with axial skeleton lesions, including vertebral, pelvic, and rib lesions, where classic radiographic signs may be absent or attenuated.
- Coordinate biopsy planning with surgery: CT-guided biopsy should be performed in consultation with the orthopedic oncologist, with the biopsy tract placed in a site that can be excised en bloc at the time of definitive surgery.
- Integrate DWI in the MRI protocol: Functional sequences including DWI and ADC mapping should be incorporated into baseline and response-assessment MRI protocols, given their established role in characterizing tumor cellularity and monitoring chemotherapy response.
- Multidisciplinary team discussion is mandatory: All cases of suspected or confirmed Ewing's sarcoma should be discussed at a dedicated bone tumor multidisciplinary team (MDT) meeting including radiology, orthopedic oncology, pediatric oncology, pathology, and radiation oncology prior to initiating treatment.

6. Limitations

This study has several inherent limitations that must be acknowledged. The primary limitation is the small sample size of five patients, reflecting the rarity of Ewing's sarcoma in clinical practice even at a tertiary care institution. The small cohort precludes meaningful statistical analysis and limits the generalizability of the findings. The retrospective design introduces the potential for selection bias, as only patients with complete imaging datasets and confirmed histopathological diagnosis were included. Not all advanced MRI sequences (e.g., dynamic contrast-enhanced MRI, MR spectroscopy) were performed uniformly across all patients due to clinical constraints. Additionally, outcome data including response to chemotherapy and overall survival were not the focus of this imaging-centric study and have therefore not been reported. Prospective multicenter studies with larger patient cohorts are needed to validate and expand upon the observations presented here.

7. Conclusion

This retrospective study of five histopathologically confirmed cases of Ewing's sarcoma demonstrates that a structured multimodal imaging approach — integrating plain radiography, CT, and MRI — is essential for achieving diagnostic confidence, accurate local staging, and informed therapeutic planning. Plain radiographs provide the critical initial diagnostic clue, particularly through identification of aggressive periosteal reaction patterns. CT excels in cortical assessment and biopsy guidance. MRI is the definitive modality for local staging, marrow extent delineation, and response monitoring.

The imaging spectrum of Ewing's sarcoma extends beyond the classical diaphyseal long bone presentation and encompasses axial sites including the vertebral column and pelvis, where awareness of site-specific imaging nuances is paramount. Recognition of characteristic but not pathognomonic imaging features,

integrated with clinical context and histopathological correlation, enables timely diagnosis and facilitates the initiation of potentially curative multimodal treatment in this aggressive pediatric malignancy.

References

1. Murphey MD, Senchak LT, Mambalam PK, Logie CI, Klassen-Fischer MK, Kransdorf MJ. Ewing sarcoma family of tumors: radiologic-pathologic correlation. Radiographics. 2013;33(3):803–31.
2. Grünewald TGP, Cidre-Aranaz F, Surdez D, et al. Ewing sarcoma. Nat Rev Dis Primers. 2018;4(1):5.
3. Delattre O, Zucman J, Plougastel B, et al. Gene fusion with an ETS DNA-binding domain caused by chromosome translocation in human tumours. Nature. 1992;359(6391):162–5.
4. Iwamoto Y. Diagnosis and treatment of Ewing's sarcoma. Jpn J Clin Oncol. 2007;37(2):79–89.
5. Daldrup-Link HE, Franzius C, Link TM, et al. Whole-body MR imaging for detection of bone metastases in children and young adults. AJR Am J Roentgenol. 2001;177(1):229–36.
6. Casali PG, Bielack S, Abecassis N, et al. Bone sarcomas: ESMO-PaedCan-EURACAN Clinical Practice Guidelines for diagnosis, treatment and follow-up. Ann Oncol. 2018;29(Suppl 4):iv79–95.
7. Andreou D, Bielack SS, Carrle D, et al. The influence of tumor- and treatment-related factors on the development of local recurrence in osteosarcoma after adequate surgery. Ann Oncol. 2011;22(5):1243–8.
8. Bernstein M, Kovar H, Paulussen M, et al. Ewing's sarcoma family of tumors: current management. Oncologist. 2006;11(5):503–19.
9. Cotterill SJ, Ahrens S, Paulussen M, et al. Prognostic factors in Ewing's tumor of bone: analysis of 975 patients from the European Intergroup Cooperative Ewing's Sarcoma Study Group. J Clin Oncol. 2000;18(17):3108–14.
10. Llauger J, Palmer J, Amores S, Bague S, Camins A. Primary tumors of the sacrum: diagnostic imaging. AJR Am J Roentgenol. 2000;174(2):417–24.
11. Goo HW, Choi SH, Ghim T, Moon HN, Seo JJ. Whole-body MRI of paediatric malignant tumours: comparison with conventional oncological imaging methods. Pediatr Radiol. 2005;35(8):766–73.
12. Esiashvili N, Goodman M, Marcus RB Jr. Changes in incidence and survival of Ewing sarcoma patients over the past 3 decades: Surveillance Epidemiology and End Results data. J Pediatr Hematol Oncol. 2008;30(6):425–30.
13. Franzius C, Sciuk J, Daldrup-Link HE, Jürgens H, Schober O. FDG-PET for detection of osseous metastases from malignant primary bone tumours: comparison with bone scintigraphy. Eur J Nucl Med. 2000;27(9):1305–11.
14. Hoffer FA. Biopsy. In: Kirks DR, Griscom NT, editors. Practical Pediatric Imaging. 3rd ed. Philadelphia: Lippincott-Raven; 1998. p. 467–75.
15. Bacci G, Ferrari S, Bertoni F, et al. Prognostic factors in nonmetastatic Ewing's sarcoma of bone treated with adjuvant chemotherapy: analysis of 359 patients at the Istituto Ortopedico Rizzoli. J Clin Oncol. 2000;18(1):4–11.
16. American College of Radiology. ACR Appropriateness Criteria: Primary Bone Tumors. Reston: ACR; 2020 [cited 2024 Nov]. Available from: https://www.acr.org/Clinical-Resources/ACR-Appropriateness-Criteria
17. Schuetze SM, Rubin BP, Vernon C, et al. Use of positron emission tomography in localized extremity soft tissue sarcoma treated with neoadjuvant chemotherapy. Cancer. 2005;103(2):339–48.

18. Verstraete KL, Lang P. Bone and soft tissue tumors: the role of contrast agents for MR imaging. Eur J Radiol. 2000;34(3):229–46.
19. Subhawong TK, Jacobs MA, Fayad LM. Insights into quantitative diffusion-weighted MRI for musculoskeletal tumor imaging. AJR Am J Roentgenol. 2014;203(3):560–72.
20. Byun BH, Kong CB, Lim I, et al. Combination of 18F-FDG PET/CT and diffusion-weighted MR imaging as a predictor of histologic response to neoadjuvant chemotherapy: preliminary results in osteosarcoma. J Nucl Med. 2013;54(7):1053–9.
21. Enneking WF, Spanier SS, Goodman MA. A system for the surgical staging of musculoskeletal sarcoma. Clin Orthop Relat Res. 1980;(153):106–20.
22. Ozaki T, Flege S, Kevric M, et al. Osteosarcoma of the spine: experience of the Cooperative Osteosarcoma Study Group. Cancer. 2002;94(4):1069–77.
23. Meyer JS, Dormans JP. Differential diagnosis of pediatric musculoskeletal masses. Magn Reson Imaging Clin N Am. 1998;6(3):561–77.
24. Juergens C, Weston C, Lewis I, et al. Safety assessment of intensive induction with vincristine, ifosfamide, doxorubicin, and etoposide (VIDE) in the treatment of Ewing tumors in the EURO-E.W.I.N.G. 99 clinical trial. Pediatr Blood Cancer. 2006;47(1):22–9.
25. Picci P, Bohling T, Bacci G, et al. Chemotherapy-induced tumor necrosis as a prognostic factor in localized Ewing's sarcoma of the extremities. J Clin Oncol. 1997;15(4):1553–9.